

Identifying Slowly-Varying and Turbulent Wind Features for Flight Loads Analyses

July 1999

Prepared by

C. E. SPIEKERMANN, B. H. SAKO, A. M. KABE
Structural Dynamics Department

Prepared for

SPACE AND MISSILE SYSTEMS CENTER
AIR FORCE MATERIEL COMMAND
2430 E. El Segundo Boulevard
Los Angeles Air Force Base, CA 90245

Contract No. F04701-93-C-0094

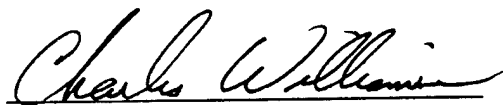
Engineering and Technology Group

APPROVED FOR PUBLIC RELEASE;
DISTRIBUTION UNLIMITED

This report was submitted by The Aerospace Corporation, El Segundo, CA 90245-4691, under Contract No. F04701-93-C-0094 with the Space and Missile Systems Center, P. O. Box 92960, Los Angeles, CA 90009-2960. It was reviewed and approved for The Aerospace Corporation by R. W. Fillers, Principal Director. The project officer is Maj. Charles R. Williamson.

This report has been reviewed by the Public Affairs Office (PAS) and is releasable to the National Technical Information Service (NTIS). At NTIS, it will be available to the general public, including foreign nationals.

This technical report has been reviewed and is approved for publication. Publication of this report does not constitute Air Force approval of the report's findings or conclusions. It is published only for the exchange and stimulation of ideas.

A handwritten signature in cursive script, reading "Charles R. Williamson", is written over a horizontal line.

Maj. Charles R. Williamson
Project Officer

REPORT DOCUMENTATION PAGEForm Approved
OMB No. 0704-0188

Public reporting burden for this collection of information is estimated to average 1 hour per response, including the time for reviewing instructions, searching existing data sources, gathering and maintaining the data needed, and completing and reviewing the collection of information. Send comments regarding this burden estimate or any other aspect of this collection of information, including suggestions for reducing this burden, to Washington Headquarters Services, Directorate for Information Operations and Reports, 1215 Jefferson Davis Highway, Suite 1204, Arlington, VA 22202-4302, and to the Office of Management and Budget, Paperwork Reduction Project (0704-0188), Washington, DC 20503.

1. AGENCY USE ONLY (Leave blank)		2. REPORT DATE July 1999	3. REPORT TYPE AND DATES COVERED Final	
4. TITLE AND SUBTITLE Identifying Slowly-Varying and Turbulent Wind Features for Flight Loads Analyses			5. FUNDING NUMBERS F04701-93-C-0094	
6. AUTHOR(S) C. E. Spiekermann, B. H. Sako, A. M. Kabe				
7. PERFORMING ORGANIZATION NAME(S) AND ADDRESS(ES) The Aerospace Corporation 2350 E. El Segundo Boulevard El Segundo, CA 90245			8. PERFORMING ORGANIZATION REPORT NUMBER TR-99(1534)-2	
9. SPONSORING/MONITORING AGENCY NAME(S) AND ADDRESS(ES) Space and Missile Systems Center Air Force Materiel Command 2430 E. El Segundo Boulevard Los Angeles Air Force Base, CA 90245			10. SPONSORING/MONITORING AGENCY REPORT NUMBER SMC-TR-00-21	
11. SUPPLEMENTARY NOTES				
12a. DISTRIBUTION/AVAILABILITY STATEMENT Approved for public release; distribution unlimited			12b. DISTRIBUTION CODE	
13. ABSTRACT (Maximum 200 words) A methodology developed to determine the spectral boundary between the slowly-varying components and the more rapidly varying, or turbulent components, of measured wind profiles is presented. Pairs of measured wind velocity versus altitude profiles from the Eastern and Western launch ranges of the United States were used to establish the vertical wavelengths which could no longer be considered slowly varying over discrete time intervals. Analyses were performed for wind pairs that were 30, 60, 90, and 120 minutes apart. The wavelength boundary between slowly-varying and turbulent wind features as a function of time interval is presented. The results of this work make it now possible to identify and extract the slowly-varying and/or turbulent wind features, as needed for a specific day-of-launch flight loads analysis, for these two launch facilities.				
14. SUBJECT TERMS Day-of-launch, winds, coherence, turbulence, loads			15. NUMBER OF PAGES 42	
			16. PRICE CODE	
17. SECURITY CLASSIFICATION OF REPORT Unclassified	18. SECURITY CLASSIFICATION OF THIS PAGE Unclassified	19. SECURITY CLASSIFICATION OF ABSTRACT Unclassified	20. LIMITATION OF ABSTRACT	

Abstract

A methodology is developed to determine the spectral boundary between wind features that can be considered slowly varying, and the more rapidly-varying, or turbulent, features of measured wind profiles. Pairs of measured wind velocity versus altitude profiles from the Eastern and Western launch ranges of the United States were used to establish the vertical wavelengths which could no longer be considered slowly varying over discrete time intervals. Analyses were performed for wind pairs that were 30, 60, 90 and 120 minutes apart. The wavelength boundary between slowly-varying and turbulent wind features as a function of time interval is presented. The results of this work make it possible to identify and extract the slowly-varying and turbulent wind features at a particular launch site.

Contents

Abstract.....	1
Acknowledgments	7
Nomenclature	9
1. Introduction	11
2. Procedure.....	13
3. Overview of Study	15
4. Results	25
5. Potential Uses.....	37
6. Conclusions	39
References	41

Figures

1.	Example profile of a 30-minute wind pair from Eastern Range measured 870318 at 1630z and 1700z	11
2.	Example profile of a 90-minute wind pair from Eastern Range measured 870318 at 1630z and 1800z	12
3.	Example power spectral density of a 30-minute wind pair from Eastern Range measured 870318 at 1630z and 1700z	18
4.	Example power spectral density of a 90-minute wind pair from Eastern Range measured 870318 at 1630z and 1800z	18
5.	Example of coherence squared of 30-minute wind pair from ER measured 870318 at 1630z and 1700z	19
6.	Example of coherence squared of 90-minute wind pair from ER measured 870318 at 1630z and 1800z	20
7.	Range sum test for 30-minute pairs.....	21
8.	Range sum test for 60-minute pairs.....	21
9.	Range sum test for 90-minute pairs.....	22
10.	Range sum test for 120-minute pairs.....	22
11.	Distribution of 30-minute wind pairs boundary wavenumbers.....	25
12.	Distribution of 60-minute wind pairs boundary wavenumbers.....	26
13.	Distribution of 90-minute wind pairs boundary wavenumbers.....	26
14.	Distribution of 120-minute wind pairs boundary wavenumbers.....	27
15.	Distribution of 30-minute wind pairs boundary wavelengths	28
16.	Distribution of 60-minute wind pairs boundary wavelengths	28
17.	Distribution of 90-minute wind pairs boundary wavelengths	29
18.	Distribution of 120-minute wind pairs boundary wavelengths	29
19.	Average coherence spectrum from 79 wind pairs measured 30 minutes apart.....	31
20.	Average coherence spectrum from 106 wind pairs measured 60 minutes apart.....	32
21.	Average coherence spectrum from 187 wind pairs measured 90 minutes apart.....	33
22.	Average coherence spectrum from 180 wind pairs measured 120 minutes apart	34
23.	Average wavelength boundary separating the slowly-varying and turbulent components of winds as a function of elapsed time	35

Table

1.	Monthly Distribution of Wind Pairs Evaluated from Both ER and WR.....	15
2.	Yearly Distribution of Wind Pairs Evaluated from Both ER and WR	16
3.	Winter Months Distribution of Wind Pairs Evaluated from ER and WR.....	23
4.	Boundary Wavelengths Between Slowly-Varying and Turbulent Atmospheric Wind Wavelengths.....	27

Acknowledgments

The authors are grateful to Dr. J. M. Womack of The Aerospace Corporation for his assistance in evaluating the statistical similarity of the coherence boundary wavenumbers, and for performing the Rank Sum Test that established that the ER and WR boundary wavelengths for the winter months can be treated as part of a single statistical family. Gratitude is also expressed to Dr. R. Walterscheid of The Aerospace Corporation for his helpful suggestions during several discussions regarding spectral analysis of wind data.

Nomenclature

A	indicates first measurement of a wind pair
B	indicates second measurement of a wind pair
f	wind vertical wavenumber, cycles/ft
$f_{n,\Delta T}$	boundary wavenumber for $n^{\text{th}} \Delta T$ wind pair
$f_{\text{ave},\Delta T}$	boundary wavenumber for average ΔT coherence
\hat{G}_{u,u_A}	Power Spectral Density of A wind u-component, $\text{ft}^3 \text{s}^{-2} \text{ cycle}^{-1}$
\hat{G}_{u,u_B}	Cross Spectral Density wind u-components, $\text{ft}^3 \text{s}^{-2} \text{ cycle}^{-1}$
$N_{\Delta T}$	number of wind pairs with time interval ΔT
n	n^{th} wind pair, $n = 1, 2, \dots, N_{\Delta T}$
u	zonal (west, east) component of wind
v	meridional (south, north) component of wind
^	indicates estimated parameter
$\hat{\Gamma}_{u,u_A}^2$	coherence-square for wind pair u-components
$\hat{\Gamma}_{n,\Delta T}^2$	weighted u,v coherence-square for $n^{\text{th}} \Delta T$ wind pair
$\hat{\Gamma}_{\text{ave},\Delta T}^2$	average coherence-square across all ΔT wind pairs
ΔT	time interval between wind measurements, min
λ	atmospheric wind vertical wavelength, ft
$\lambda_{\text{ave},\Delta T}$	wavelength corresponding to $f_{\text{ave},\Delta T}$, ft
$\lambda_{n,\Delta T}$	boundary wavelength corresponding to $f_{n,\Delta T}$, ft
$\bar{\lambda}_{n,\Delta T}$	mean boundary wavelength, all ΔT wind pairs, ft
$\sigma_{n,\Delta T}$	standard deviation of boundary wavelengths, ft

1. Introduction

Aerodynamic pressure acting on a launch vehicle during atmospheric flight is a significant source of structural loading.^{1,2} This loading is greatly influenced by the atmospheric wind through which the vehicle flies.³⁻⁶ Loads analyses are typically divided into those that can be performed just prior to launch and those that have to be completed prior to the day of launch.^{7,8} Both sets of loads are then combined statistically just prior to launch to estimate the total vehicle loads that are then compared to the allowable values.^{9,12}

A vertical wavelength can be thought of as an altitude-dependent wind feature which modulates the angle of attack of a launch vehicle as it flies through the wind. There may be many spectral components of various vertical wavelengths present within any altitude sample of a wind profile. Spectral analysis is possible, where the independent variable is altitude. Loads calculations performed on the day of launch are reasonable for that portion of the load that is associated with the slowly-varying vertical wavelengths in the wind velocity versus altitude profile. Typical wind profiles containing both the slowly-varying and the turbulent features of the wind are shown in Figs. 1 and 2 for a pair of balloon measurements.

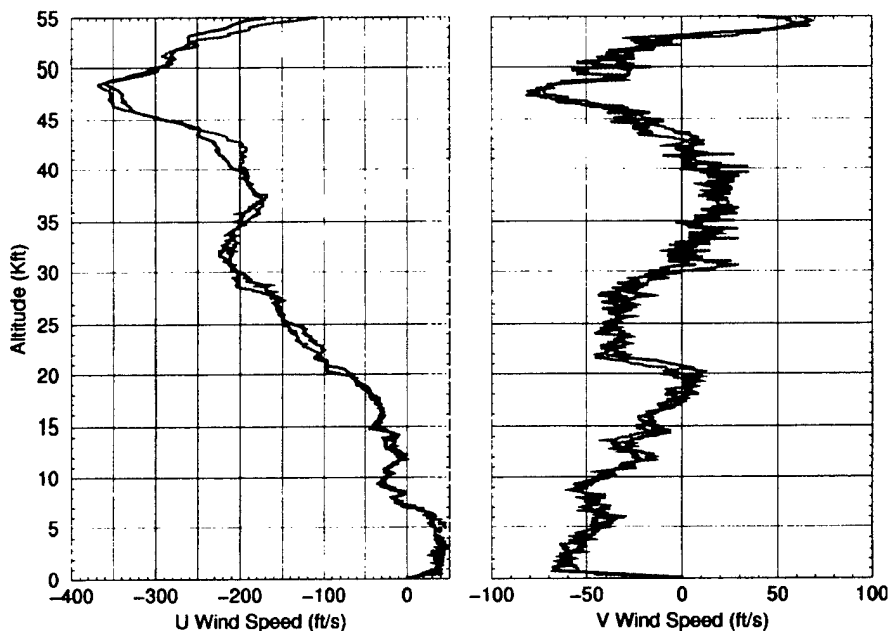


Figure 1. Example profile of a 30-minute wind pair from Eastern Range measured 870318 at 1630z and 1700z. U (west, east) component on left and V (south, north) component on right show longer vertical wavelengths persistent over this time period.

It is intuitive that longer vertical wavelengths are more slowly varying over time than shorter wavelengths. It is evident in Figs. 1 and 2 that the longer vertical wavelengths are more slowly

varying and that the shorter vertical wavelengths vary much more over time. The variation is more evident as the time interval increases from 30 minutes to 90 minutes in Figs. 1 and 2. Loads due to the rapidly-varying, or turbulent, components of the wind should be treated statistically and independent of the measured day-of-launch wind. To do this, it is critical that the boundary between the slowly and rapidly-varying components of the wind be identified.

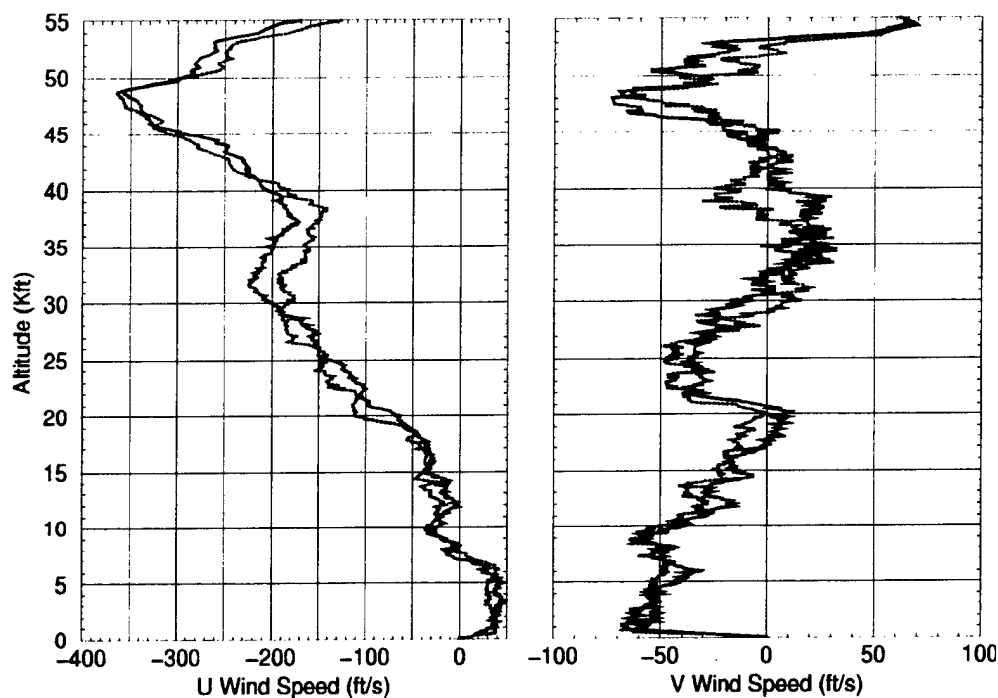


Figure 2. Example profile of a 90-minute wind pair from Eastern Range measured 870318 at 1630z and 1800z. Fewer long vertical wavelengths are persistent compared to the previous 30-minute wind pair.

2. Procedure

The coherence-squared function applied to wind pairs form the basis here for determining the wavenumber, f , which defines the spectral boundary between the slowly-varying and the turbulent wind features. A wavenumber¹³ represents the number of waves of a particular wavelength in a unit distance. A wavenumber is also the inverse of the wavelength, λ , the distance between two successive crests of a single periodic component in the vertical wind profile. Denote (U_A, V_A) to be the zonal (u, west-east) and meridional (v, south-north) components of the "A-wind" measured at some given instance; and (U_B, V_B) to be the "B-wind," occurring ΔT minutes later. In day-of-launch operations, the A-wind will be known from measurements, and the unknown B-wind is the wind profile through which the launch vehicle will fly. Therefore, the B-wind is viewed as a perturbation of the A-wind. In terms of the u-component, we would have at any altitude, h ,

$$U_B(h) = U_A(h) + N_U(h) \quad (1)$$

where, N_U is the "u-noise" component accounting for non-persistent changes in U_A . The coherence-square function for the u-component of a pair of A and B winds is defined by,

$$\Gamma_{U_A U_B}^2(f) = \frac{|G_{U_A U_B}(f)|^2}{G_{U_A U_A}(f) G_{U_B U_B}(f)} \quad (2)$$

where, $G_{U_A U_B}$, is the cross spectral density (CSD) function of U_A and U_B ; and $G_{U_A U_A}$ and $G_{U_B U_B}$ are the power spectral density (PSD) functions of U_A and U_B , respectively.

If we assume that N_U is uncorrelated to U_A , then Eq. (2) simplifies to

$$\Gamma_{U_A U_B}^2(f) = \frac{1}{1 + G_{N_U N_U}(f)/G_{U_A U_A}(f)} \quad (3)$$

which gives a coherence-squared value of 0.5 for a signal-to-noise ratio of 1. Since longer wavelength wind features are more slowly varying, we would expect $\Gamma_{U_A U_B}^2$ to be monotonically decreasing with wavenumber, f . Therefore, the wavenumber for which the coherence-square value is equal to 0.5 will be used here to define the spectral boundary between the slowly-varying and turbulent wind features.

Similarly, define the coherence-squared function for the v-component of a pair of A and B winds by,

$$\Gamma_{V_A V_B}^2(f) = \frac{|G_{V_A V_B}(f)|^2}{G_{V_A V_A}(f) G_{V_B V_B}(f)} \quad (4)$$

To determine a spectral boundary between slowly-varying and turbulent wind features which is applicable to both u and v components, the coherence-squared functions in Eqs. (2) and (4) can be combined using a PSD weighted average. Specifically, let

$$\theta_U(f) = \frac{G_{U_A U_A}(f) + G_{U_B U_B}(f)}{G_{U_A U_A}(f) + G_{U_B U_B}(f) + G_{V_A V_A}(f) + G_{V_B V_B}(f)} \quad (5)$$

and,

$$\theta_V(f) = \frac{G_{V_A V_A}(f) + G_{V_B V_B}(f)}{G_{U_A U_A}(f) + G_{U_B U_B}(f) + G_{V_A V_A}(f) + G_{V_B V_B}(f)} \quad (6)$$

represent the fraction of the total energy for the u and v components, respectively. The weighted average coherence-squared function for a given wind pair is defined as,

$$\Gamma_{ave}^2 = \theta_U \cdot \Gamma_{U_A U_B}^2 + \theta_V \cdot \Gamma_{V_A V_B}^2 \quad (7)$$

The wavenumber, f , determined from

$$\Gamma_{ave}^2(f) = 0.5 \quad (8)$$

is taken to be the boundary which spectrally separates the slowly-varying and turbulent wind features.

Computation of the coherence-squared function is accomplished using the Discrete Fourier Transform (DFT) as described in Bendat and Piersol.¹⁴ For each wind pair, only winds corresponding to altitudes between 5K ft and 50K ft were used. Estimation of the CSD and PSD which appear in the numerator and denominator of Eqs. (2) and (4) was performed using a 50 percent overlapping process with a DFT block size corresponding to 10K ft. Additionally, each data block had its mean removed and was tapered using a Hanning window prior to applying the DFT.

3. Overview of Study

Measured wind profiles, consisting of wind speed and direction as a function of altitude in 100-foot increments from approximately the ground to approximately 50,000 ft, were gathered from an extensive historical winds database. These profiles are typically displayed as the zonal and the meridional wind magnitude components (Fig. 1). Only wind profiles measured with Jimsphere balloons were used since they are known to have better vertical resolution than Windsonde balloons, the other common measurement system.¹⁵⁻¹⁸ Wind profiles with significant data gaps were excluded from this study.

The winds represented all months of the year dating back to 1964 at both the Eastern Range (ER) in Florida, and the Western Range (WR) at Vandenberg Air Force Base in California (Tables 1, 2). Wind pairs were identified where the time interval between the measured wind profiles, ΔT , was 30, 60, 90, and 120 minutes (± 5 minutes for each) (Table 1). These are the range of time intervals typically used during day-of-launch operations. There were 1134 wind pairs identified.

Table 1. Monthly Distribution of Wind Pairs Evaluated from Both Eastern Range (ER) and Western Range (WR) That Were Measured 30, 60, 90, and 120 Minutes (± 5 Minutes) Apart

ΔT (min)	ER Wind Pairs					WR Wind Pairs					Total
	30	60	90	120	Sum	30	60	90	120	Sum	
January	0	3	29	24	56	10	12	14	20	56	112
February	12	17	42	42	113	4	6	14	11	35	148
March	13	11	22	28	74	2	7	9	16	34	108
April	8	14	25	26	73	20	19	7	17	63	136
May	4	6	21	17	48	4	5	14	20	43	91
June	3	4	10	11	28	0	2	11	7	20	48
July	1	6	22	23	52	0	4	9	10	23	75
August	5	8	31	18	62	0	1	13	8	22	84
September	0	4	37	17	58	2	2	15	7	26	84
October	1	9	20	14	44	8	13	7	6	34	78
November	4	8	22	16	50	0	4	13	15	32	82
December	1	10	23	17	51	9	10	8	10	37	88
Sum	52	100	304	253	709	59	85	134	147	425	1134

Table 2. Yearly Distribution of Wind Pairs Evaluated from Both Eastern Range (ER) and Western Range (WR) That Were Measured 30, 60, 90, and 120 Minutes (± 5 Minutes) Apart

ΔT (min)	ER Wind Pairs					WR Wind Pairs					Total
	30	60	90	120	Sum	30	60	90	120	Sum	
1964			2		2					0	2
1965		5	5	3	13			10		10	23
1966		3	4	6	13			11		11	24
1967		7	29	21	57		1	5	1	7	64
1968	1	2	24	7	34			2		2	36
1969			10	3	13					0	13
1970				1	1					0	1
1971			6		6		4		3	7	13
1972			11	13	24		1	6	1	8	32
1973			22		22					0	22
1974			27		27					0	27
1975			11		11					0	11
1976								1	7	8	8
1977			5	44	49				39	39	88
1978								2	1	3	3
1979							1			1	1
1980								1	1	2	2
1984								1		1	1
1987	23	15	110	107	255			82	64	146	401
1988			18	13	31			13	16	29	60
1989				1	1	23	22			45	46
1990		6		4	10	36	37			73	83
1991	2	3	2	1	8					0	8
1994	3	11	3	7	24					0	24
1995	14	9	9	3	35		6		6	12	47
1996	9	13	6	4	32		4		4	8	40
1997		26		15	41		9		4	13	54
Sum	52	100	304	253	709	59	85	134	147	425	1134

When initially looking at the wind profiles, it was obvious that the general trend was for vertical wavelengths to be less persistent as the time interval was increased. With a 30-minute interval, the two wind profiles typically appear somewhat similar (Fig. 1), but at larger time intervals, it becomes obvious that the vertical wavelengths are less persistent (Fig. 2). This lack-of-persistence was then quantified in the following manner.

For each wind pair, PSD analyses were performed using the method described in the previous section. The block size influences the smallest discernible wavenumber and the wavenumber resolution, while the wind profile altitude resolution determines the largest wavenumber because of the Nyquist constraint. Therefore, wavenumbers between 0.0001 and 0.005 are displayed. These correspond to wavelengths between 10,000 and 200 ft. The PSDs were reviewed for reasonableness: the linearity typically observed in the measurable wavenumber region and the start of the noise floor at roughly a 500-ft wavelength. Figures 3 and 4 are typical PSD plots of the wind profiles. The U and V wind components are approximately linear in the measurable range and reach the noise floor at a wavenumber of approximately 0.002 cycle/ft, or a wavelength of approximately 500 ft. There is little observable difference between the PSD plots of 30-minute and 90-minute wind pairs.

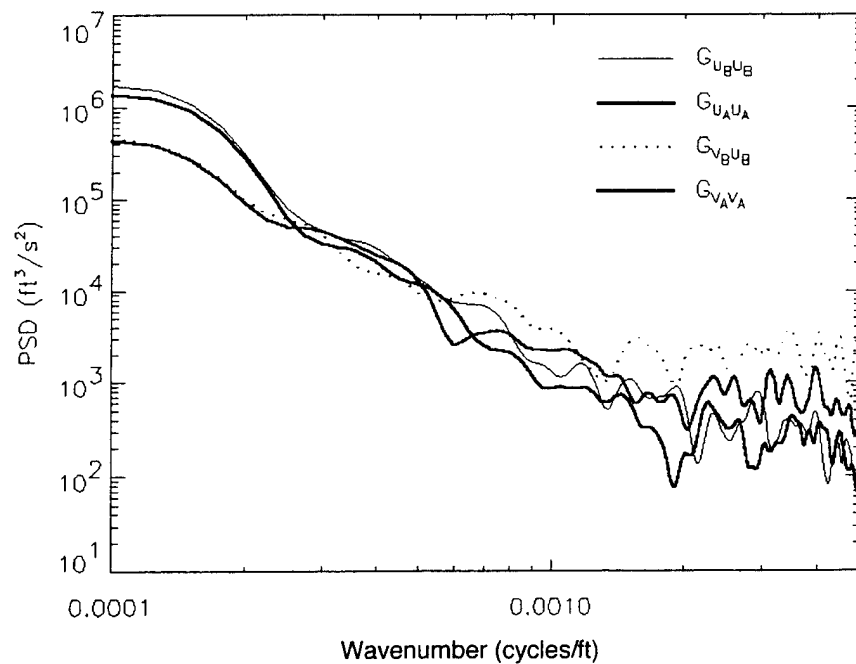


Figure 3. Example power spectral density of a 30-minute wind pair from Eastern Range measured 870318 at 1630z and 1700z. U and V wind components are linear in measurable range and reach the noise floor at approximately 0.002 cycle/foot (500 feet).

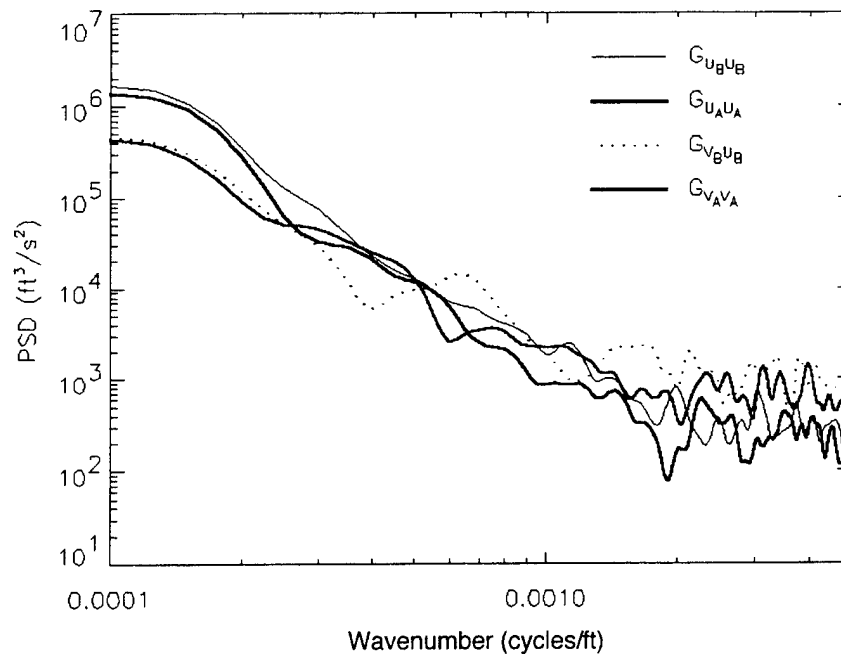


Figure 4. Example power spectral density of a 90-minute wind pair from Eastern Range measured 870318 at 1630z and 1800z. U and V wind components are linear in measurable range and reach the noise floor at approximately 0.002 cycle/foot (500 feet). Little difference is observed compared to 30-minute pair.

Next, Coherence Spectral analyses were performed on the u and the v wind components. Since these varied because of the differing energy in the u and v wind components, a single Coherence Spectrum was obtained by using the weighted average of the u and v wind components described earlier. For each Coherence Spectrum, the boundary wavenumber, $f_{n,\Delta T}$, in cycle/ft, where the weighted coherence indicated that one wind in the pair could no longer be identified from the other, was established. The coherence boundary for these wind pairs is easily identified by the weighted average coherence-squared function in Eq. (8) as

$$\hat{\Gamma}_{n,\Delta T}^2(f_{n,\Delta T}) \approx 0.5, n = 1, \dots, N_{\Delta T}, \Delta T = 30, 60, 90, 120 \quad (9)$$

Figures 5 and 6 show two examples. In Fig. 5, a 30-minute wind pair, the weighted average wind components reach a coherence-square of 0.5 at 0.000348 cycle/ft, or 2872 ft/cycle. In Fig. 6, a 90-minute wind pair, the weighted average wind components reach a coherence-square of 0.5 at 0.000202 cycle/ft, or 4950 ft/cycle.

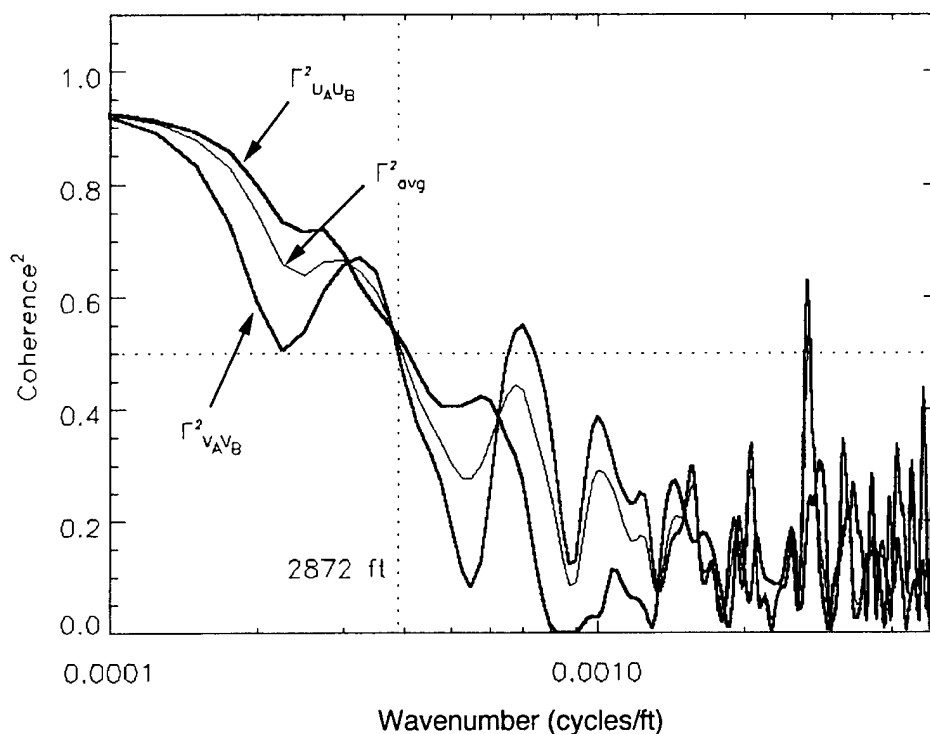


Figure 5. Example of coherence squared of 30-minute wind pair from ER measured 870318 at 1630z and 1700z. U , V , and weighted average wind components are slowly varying up to 0.000348 cycle/foot (2872 feet/cycle) boundary.

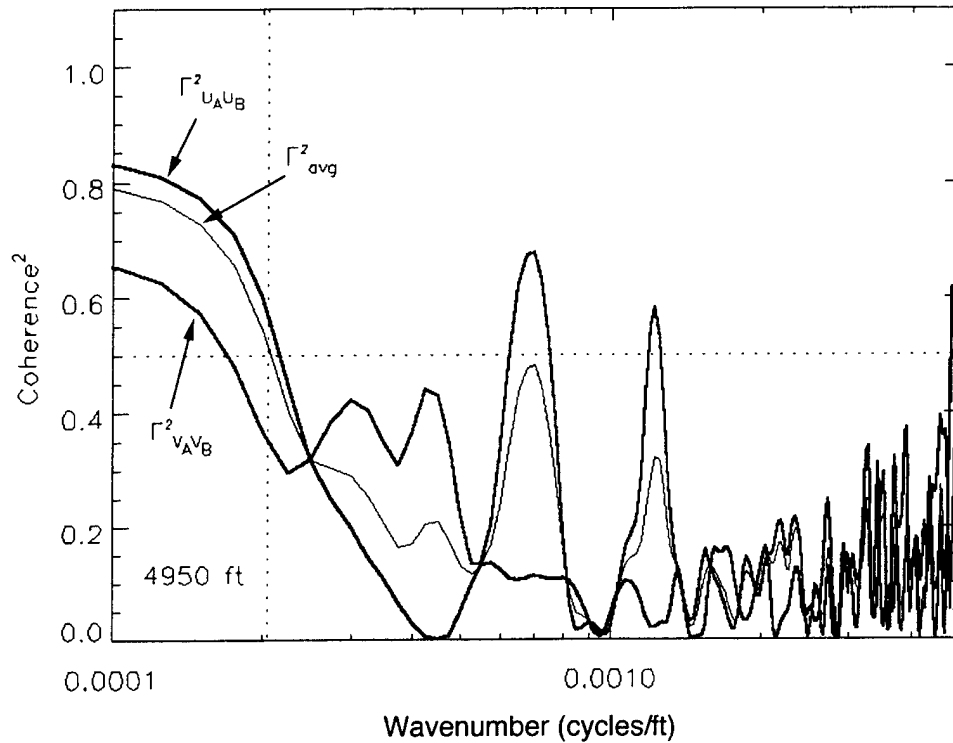


Figure 6. Example of coherence squared of 90-minute wind pair from ER measured 870318 at 1630z and 1800z. U, V, and weighted average wind components are slowly varying up to 0.000202 cycle/foot (4950) feet/cycle) boundary.

The selection of 0.5 for coherence-square is not overly harsh since it does not require complete coherence, but simply identifies the wavenumber when the incoherent portion of the wind pair becomes larger than the coherent portion. The corresponding boundary wavelength is equal to the inverse of the wavenumber, as shown in Eq. (10).

$$\lambda_{n,\Delta T} = \frac{1}{f_{n,\Delta T}}, n = 1, \dots, N_{\Delta T}, \Delta T = 30, 60, 90, 120 \quad (10)$$

A Wilcoxon Rank Sum Test¹⁹ was performed to test the hypothesis that the boundary wavelengths are statistically similar either between the ER and WR, or between the months containing winds which generally result in more severe launch vehicle loads versus the other months of the year. The months with these more severe winds are defined here as the five months, December through April. It was determined that the ER and WR severe-month wind pairs coherence boundary wavelengths could be considered to be part of the same statistical family (Figs. 7-10). However, the more severe and the other months of the year should not be considered part of the same family, for either the ER or the WR. In Figs. 7-10, the parameter T represents the sum of the ranks of one of the data sets; Z is a standardized random variable using the mean and variance of T; and P is the probability that the standardized random variable of any other partial sum of the ranks, z, is less than Z. The probabilities, P, shown in Figs. 7-10, indicate that the two data sets are statistically similar.

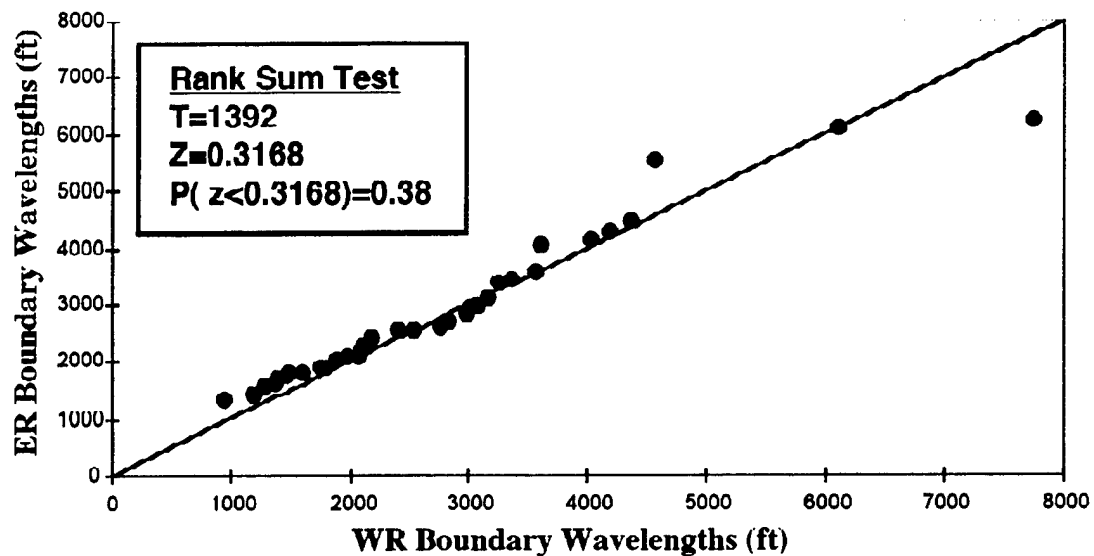


Figure 7. Rank sum test for 30-minute pairs showing ER and WR winter month boundary wavelengths can be treated as single family.

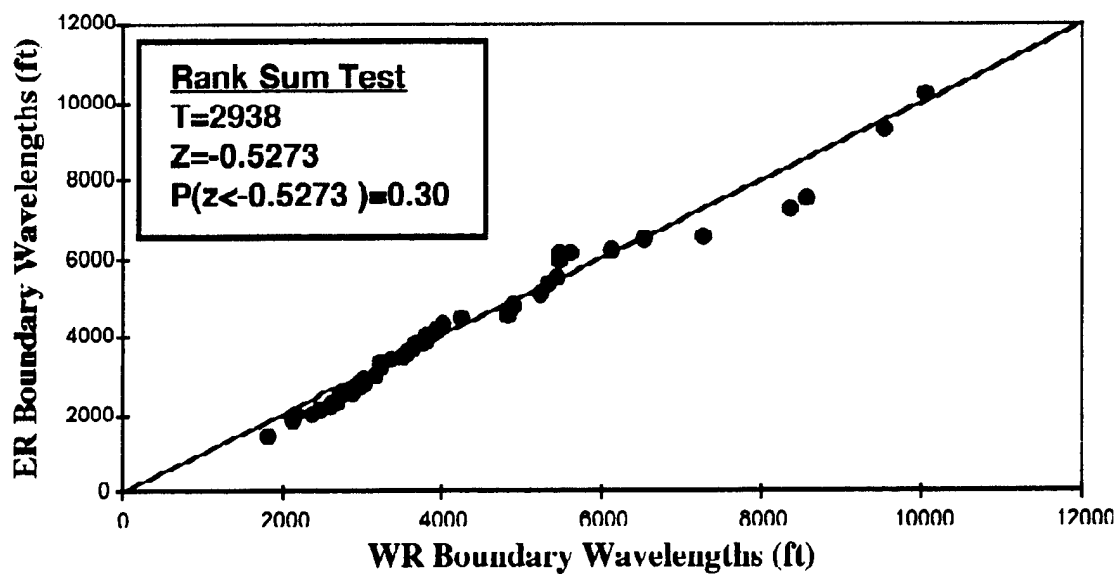


Figure 8. Rank sum test for 60-minute pairs showing ER and WR winter month boundary wavelengths can be treated as single family.

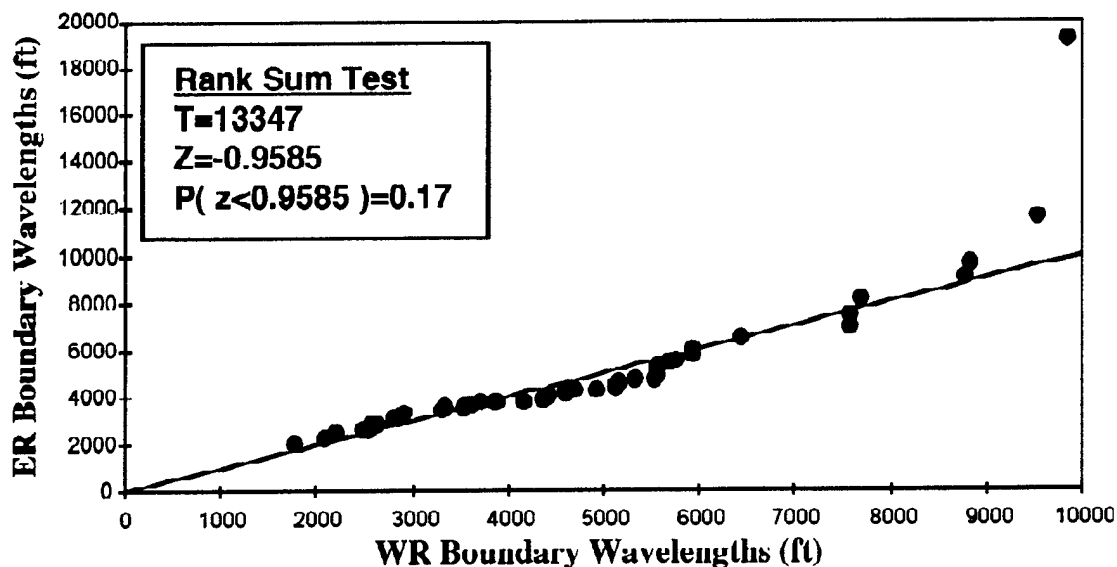


Figure 9. Rank sum test for 90-minute pairs showing ER and WR winter month boundary wavelengths can be treated as single family.

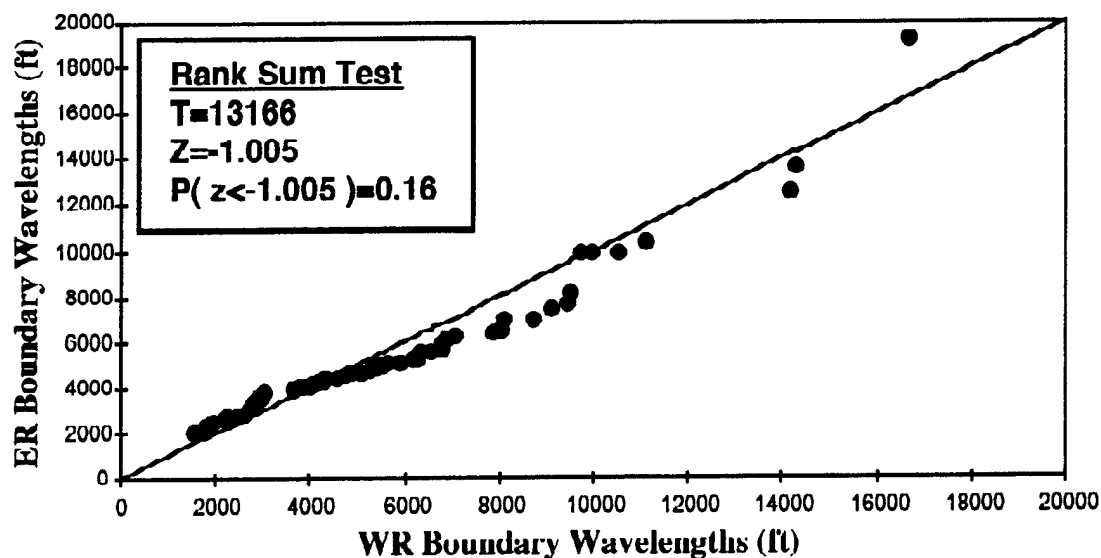


Figure 10. Rank sum test for 120-minute pairs showing ER and WR winter month boundary wavelengths can be treated as single family.

Therefore, a reasonably sized statistical sample was obtained by combining the ER and WR wind pairs from December through April. The number of wind pairs from the other months did not provide an adequate sample at all time intervals, and are not addressed here. Only the severe-months wind pairs with a boundary wavelength shorter than 10,000 ft were considered during the remainder of the study. A total of 552 wind pairs were used (Table 3).

Table 3. Winter Months Distribution of Wind Pairs Evaluated from Eastern Range (ER) and Western Range (WR). Coherence Boundaries from These Months can be Treated as Part of the Same Statistical Family.

ΔT (min)	ER Wind Pairs					WR Wind Pairs					Total
	30	60	90	120	Sum	30	60	90	120	Sum	
January	0	3	29	20	52	10	12	14	12	48	100
February	12	17	42	40	111	4	6	14	10	34	145
March	13	11	19	25	68	2	7	9	12	30	98
April	8	13	24	25	70	20	18	7	15	60	130
December	1	9	22	14	46	9	10	7	7	33	79
Sum	34	53	136	124	347	45	53	51	56	205	552

4. Results

The boundary wavenumbers obtained from Eq. (9) are displayed in histograms in Figs. 11-14 for the 30-, 60-, 90-, and 120-minute wind pairs. It is visually obvious that the mean and standard deviation of the wavenumbers decreases as the wind pair time interval increases. The specific values are presented in the figures. It is important to note that these distributions are not normal distributions. Each distribution has a positive skewness. The mean values are summarized in the left column of Table 4.

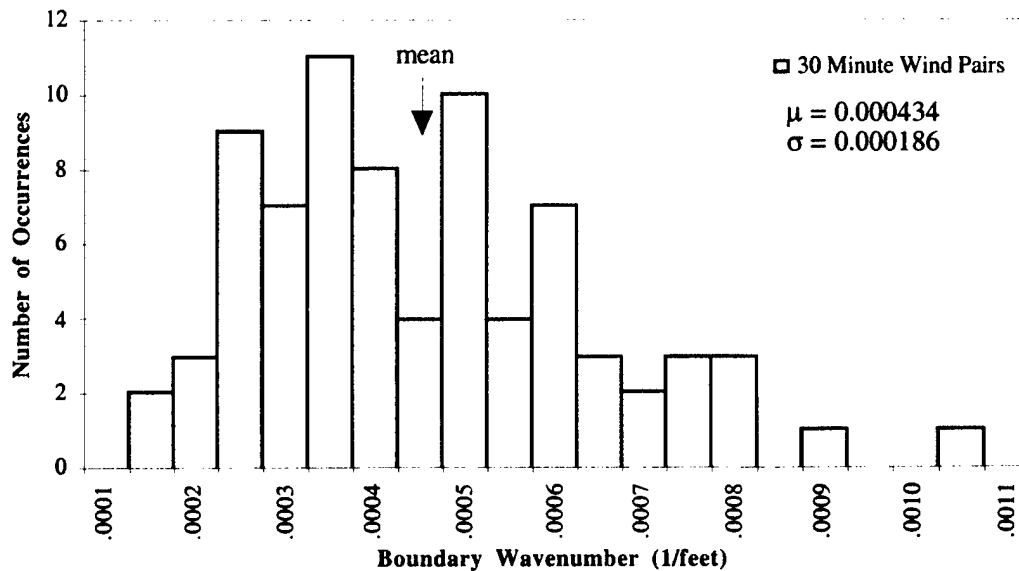


Figure 11. Distribution of the 30-minute wind pairs boundary wavenumbers.

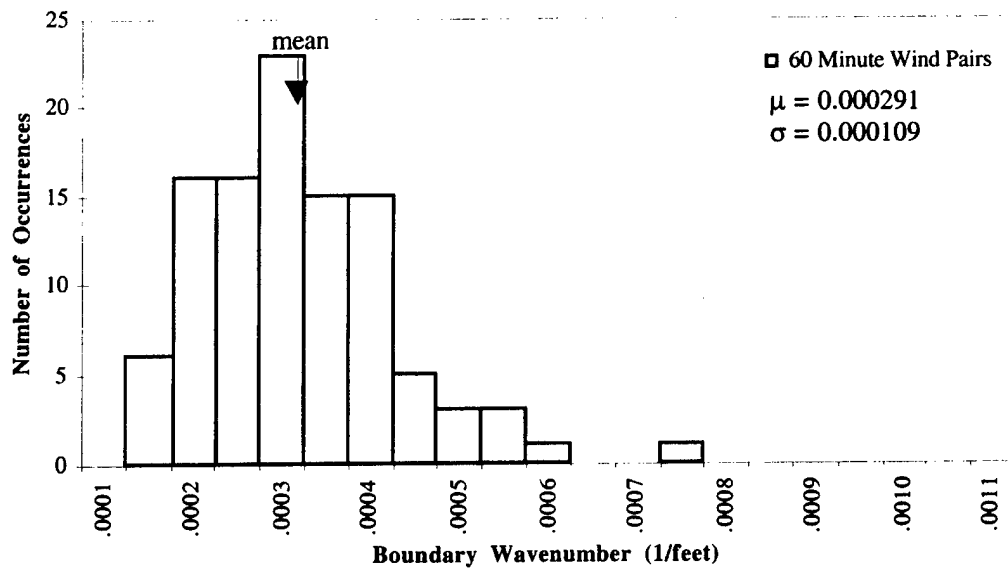


Figure 12. Distribution of the 60-minute wind pairs boundary wavenumbers.

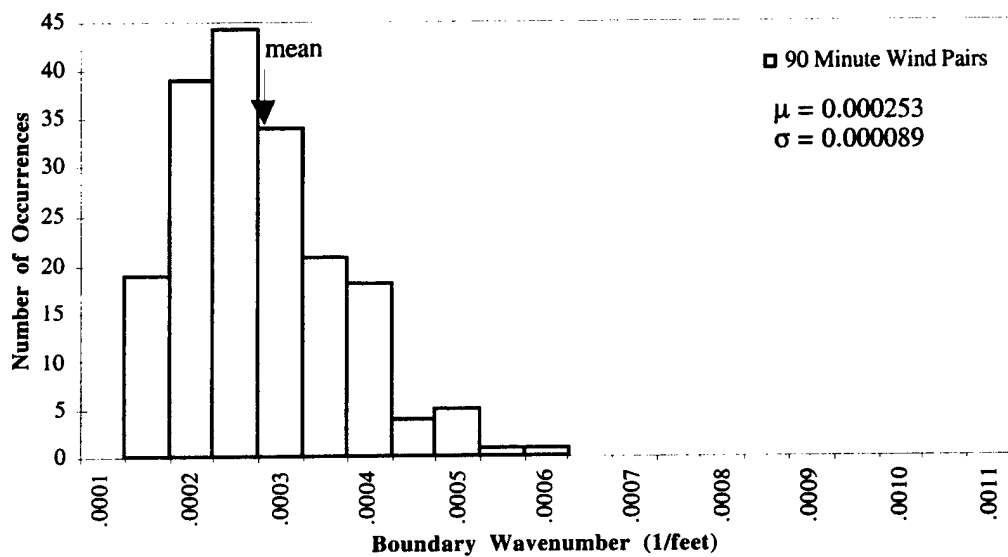


Figure 13. Distribution of the 90-minute wind pairs boundary wavenumbers.

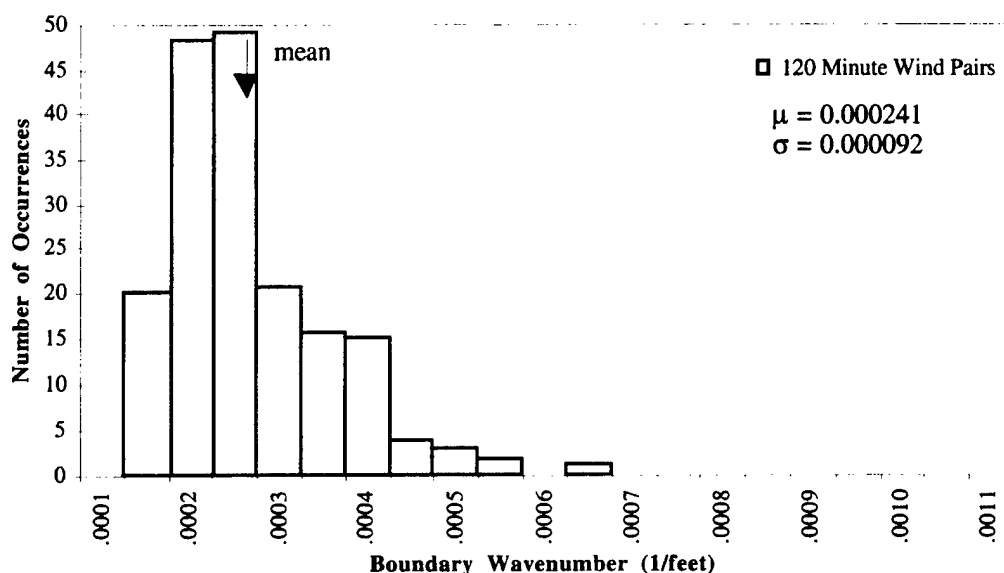


Figure 14. Distribution of the 120-minute wind pairs boundary wavenumbers.

Table 4. Boundary Wavelengths Between Slowly-Varying and Turbulent Atmospheric Wind Wavelengths. Contrasting Methods Result in Similar Values for Boundary Wavelengths

ΔT min	Boundary Wavelengths (feet)		
	from mean of wavenumbers at Coherence=0.5	from mean of (1/wavenumbers) at Coherence=0.5	from average Coherence Spectrum at Coherence=0.5
30	2304	2798	2528
60	3436	3965	3821
90	3952	4477	4346
120	4149	4725	4960

wavelength=1/wavenumber

Similarly, an alternate view of the data is obtained from the boundary wavelengths from Eq. (10), which are displayed in histograms in Figs. 15-18. As expected, the mean and standard deviation of the wavelengths increases as the wind pair time interval increases. These distributions also have a positive skewness. The wavelength means are summarized in the middle column of Table 4. The wavenumber and wavelength means for each of the time intervals would be expected to be different since the individual values are inversely related and have significant standard deviations; however, they are only approximately 15-20 percent different.

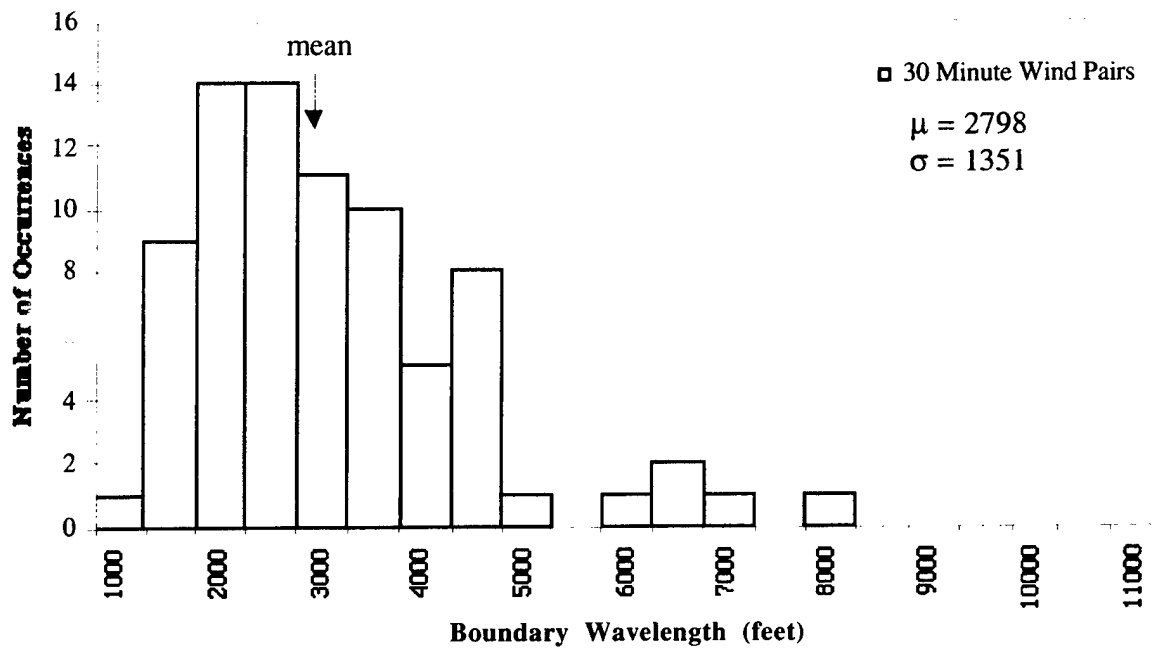


Figure 15. Distribution of the 30-minute wind pairs boundary wavelengths.

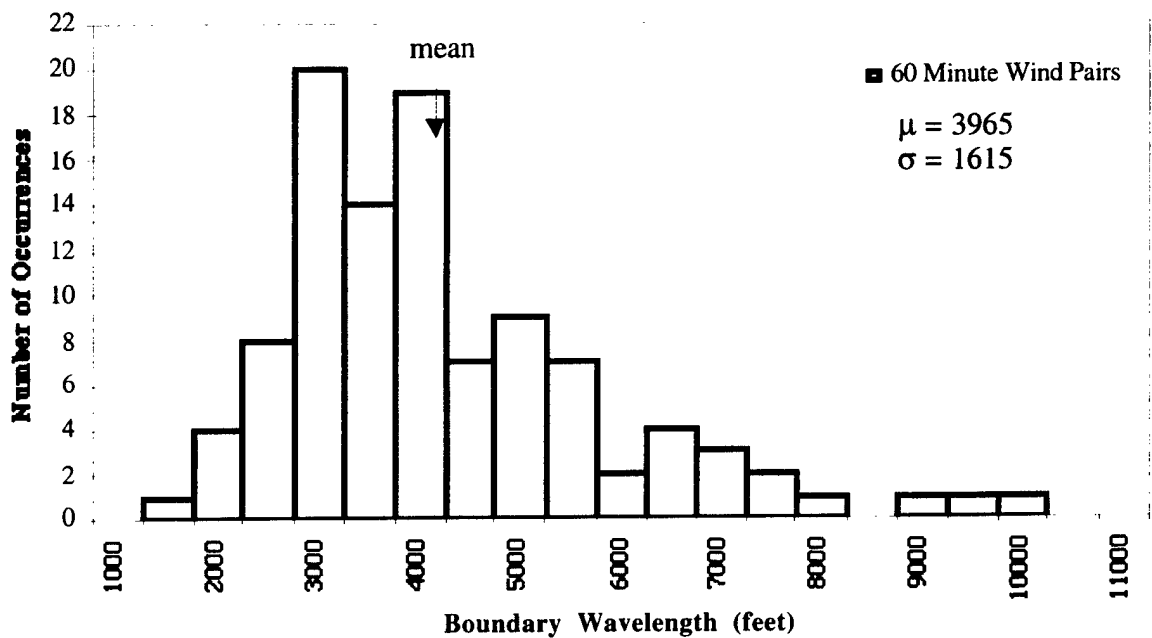


Figure 16. Distribution of the 60-minute wind pairs boundary wavelengths.

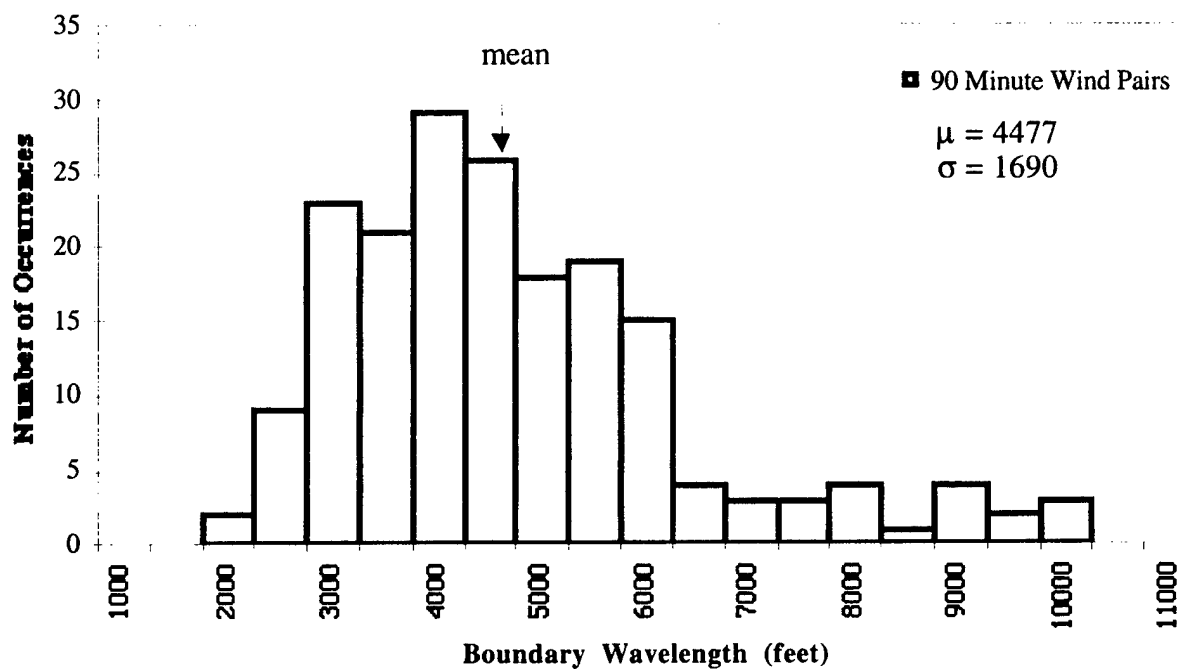


Figure 17. Distribution of the 90-minute wind pairs boundary wavelengths.

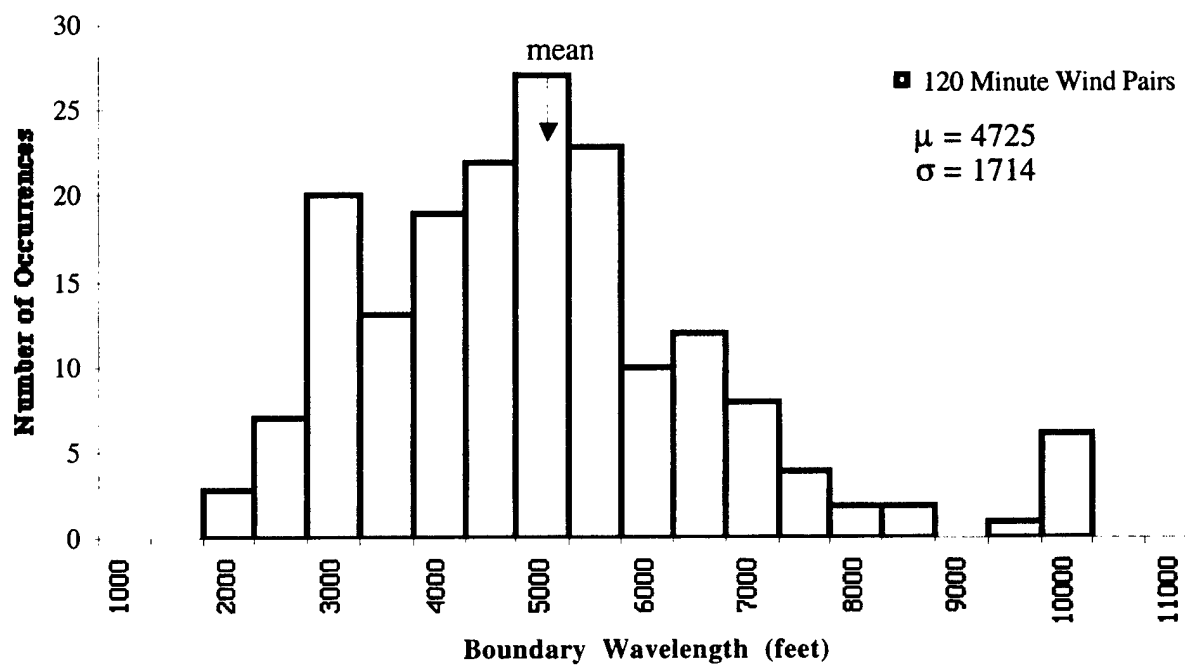


Figure 18. Distribution of the 120-minute wind pairs boundary wavelengths.

Another alternate view of the data was obtained by generating an average Coherence Spectrum from the individual Coherence Spectra for each time interval, ΔT , of 30, 60, 90 and 120 minutes.

$$\hat{\Gamma}_{ave,\Delta T}^2(f) = \frac{1}{N_{\Delta T}} \sum_{n=1}^{N_{\Delta T}} \hat{\Gamma}_{n,\Delta T}^2(f), \quad \Delta T = 30, 60, 90, 120 \quad (11)$$

From these, an average Coherence boundary wavenumber was identified for each set of wind pairs (Figs. 19-22); i.e.,

$$\hat{\Gamma}_{ave,\Delta T}^2(f_{ave,\Delta T}) \approx 0.5, \Delta T = 30, 60, 90, 120 \quad (12)$$

$$\lambda_{ave,\Delta T} = \frac{1}{f_{ave,\Delta T}}, \Delta T = 30, 60, 90, 120 \quad (13)$$

These are also presented as wavelengths in the right column of Table 4.

Wavelengths longer than those from Eq. (13) remain, on the average, slowly varying over the specified time interval. Wavelengths shorter than these values, on the average, should be considered non-persistent, and hence represent turbulence. This averaging process again resulted in boundary wavelengths similar to the previous statistical values in the first and second columns of Table 4. An advantage of this approach is that it is quantitative and minimizes engineering judgment. Plots of Eqs. (12)-(13) are shown in Figs. 19-22. The 30-minute wind pairs reach an average coherence-square of 0.5 at a wavelength of 2528 ft, the 60-minute wind pairs at 3821 ft, the 90-minute wind pairs at 4346 ft, and the 120-minute wind pairs at 4960 ft. The plus and minus one standard deviation curves in Figs. 19-22 indicate the variation in the coherence-squared, and should not be used to establish the variance of the wavelengths.

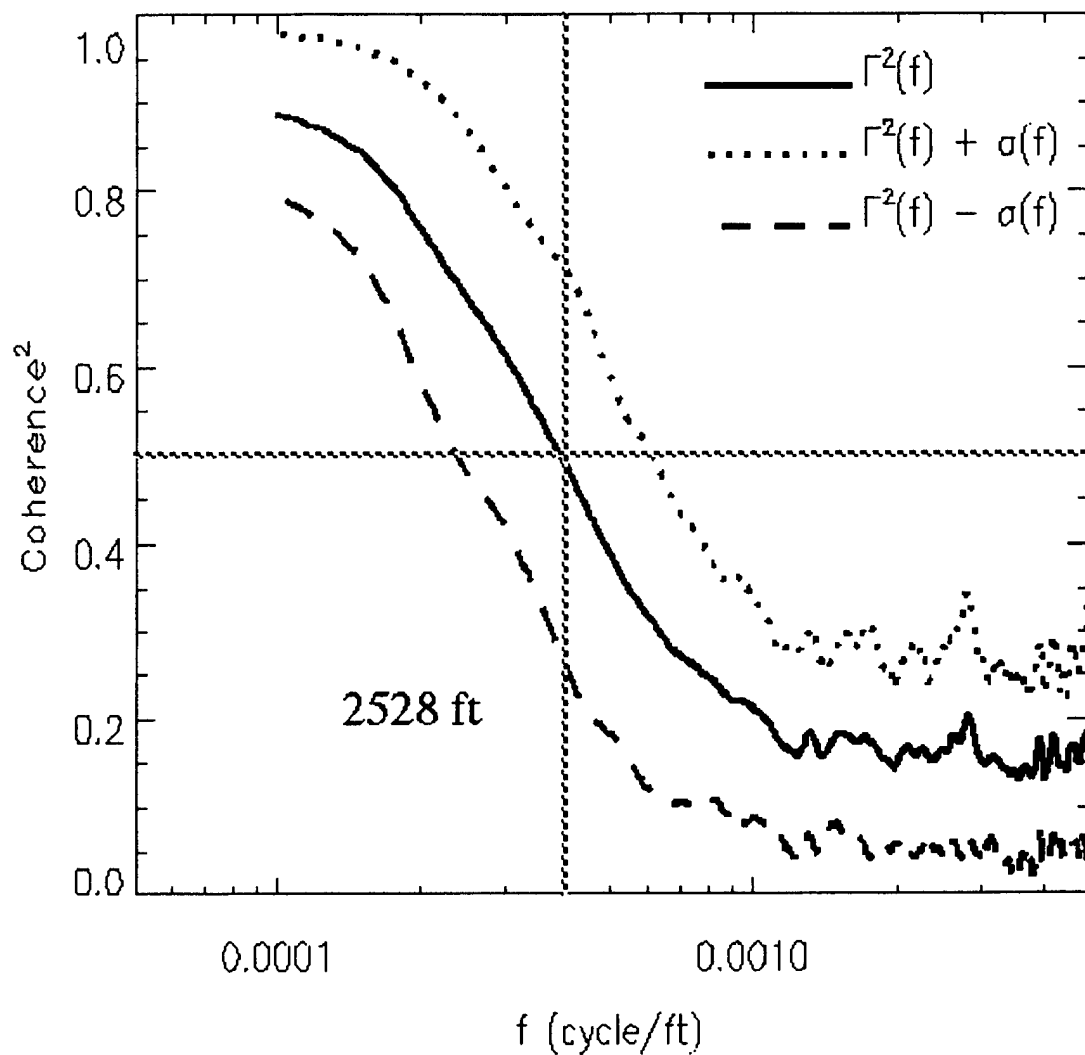


Figure 19. Average coherence spectrum from 79 wind pairs measured 30 minutes apart. Weighted average wind components are considered coherent up to the 0.00396 cycle/foot (2528 feet/cycle) boundary.

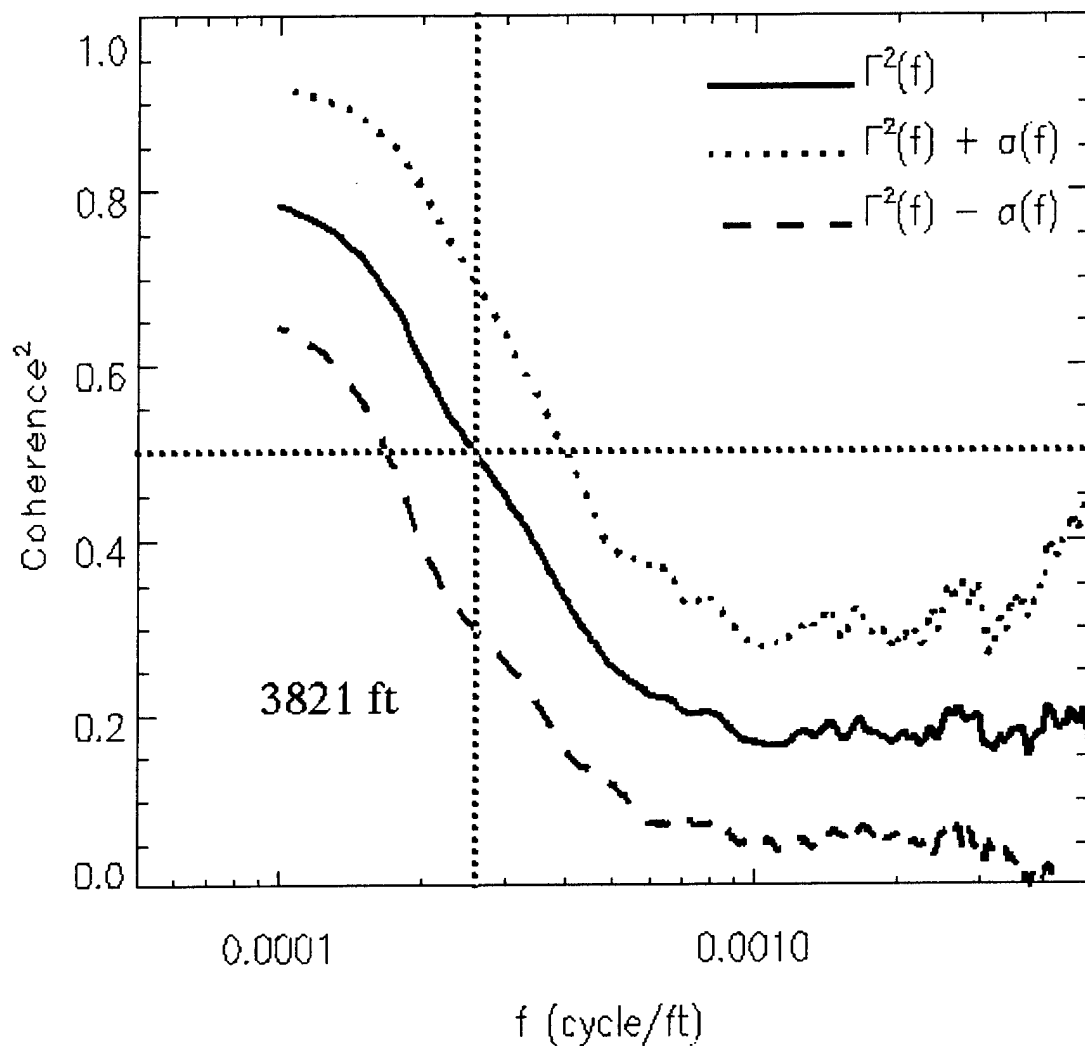


Figure 20. Average coherence spectrum from 106 wind pairs measured 60 minutes apart.
 Weighted average wind components are considered coherent up to the 0.000262
 cycle/foot (3821 feet/cycle) boundary.

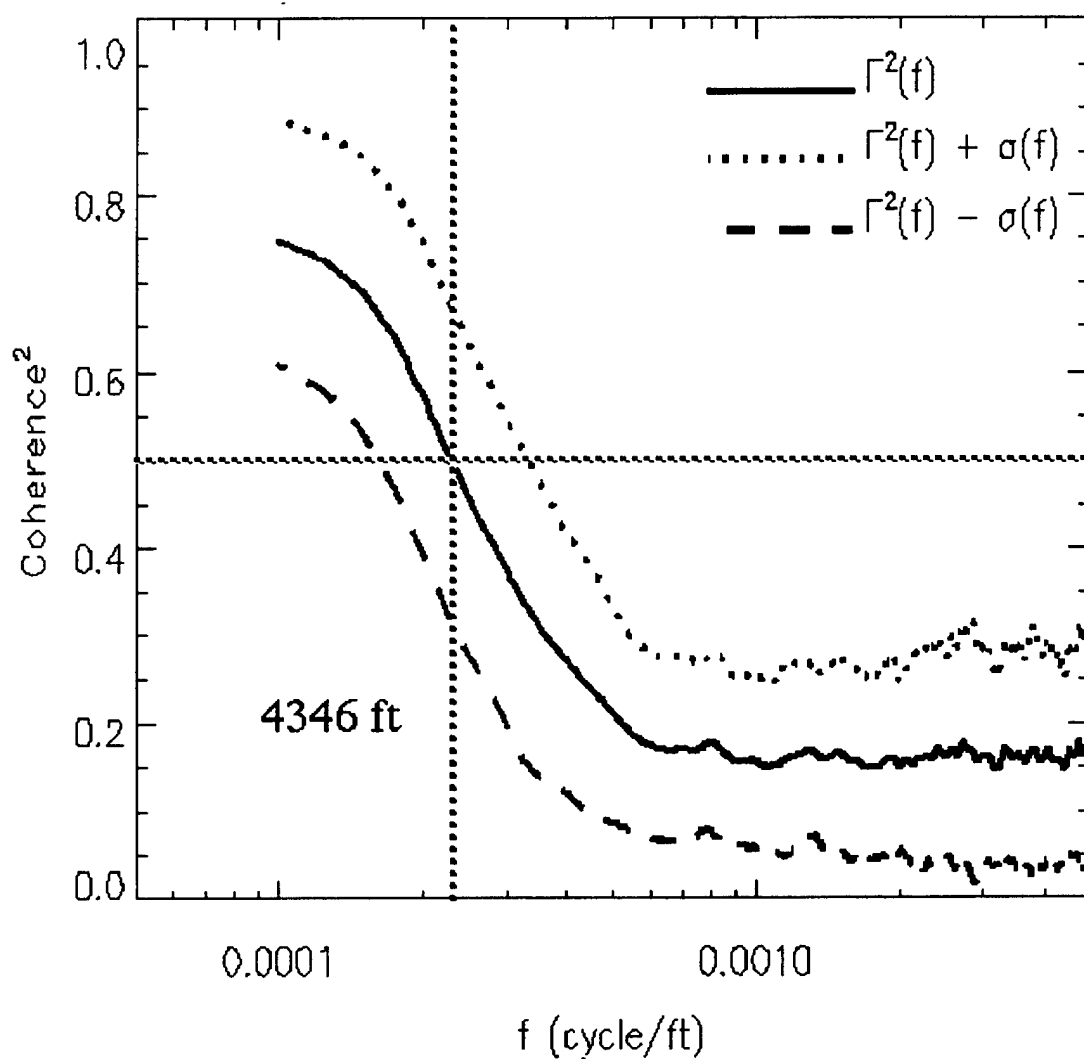


Figure 21. Average coherence spectrum from 187 wind pairs measured 90 minutes apart. Weighted average wind components are considered coherent up to the 0.000230 cycle/foot (4346 feet/cycle) boundary.

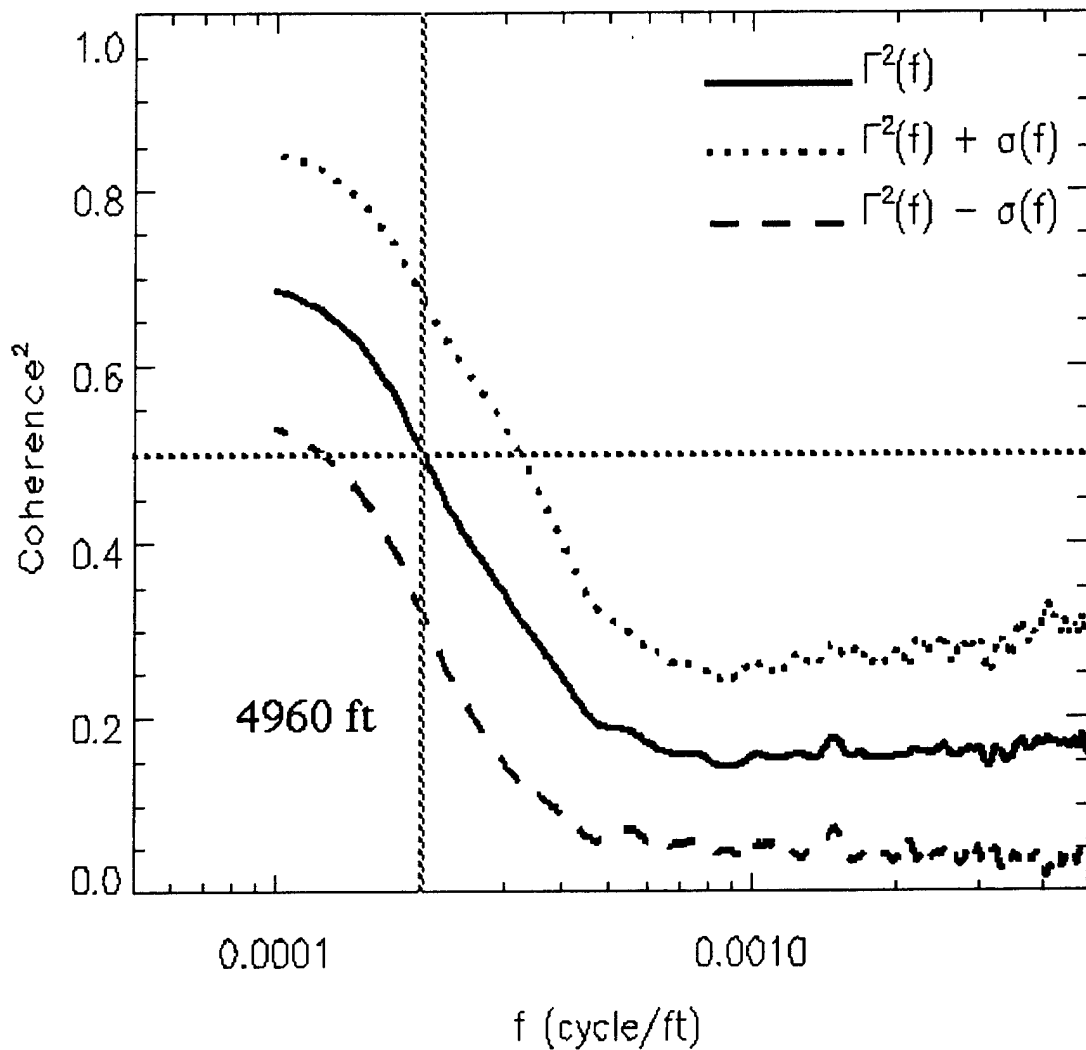


Figure 22. Average coherence spectrum from 180 wind pairs 120 minutes apart. Weighted average wind components are considered coherent up to the 0.000202 cycle/foot (4960 feet/cycle) boundary.

Finally, a curve (Fig. 23) was fit through the four average Coherence boundary wavelengths from the right column of Table 4 plus the origin, since at $\Delta T=0$ the wind pair should be coherent. An excellent fit of the data was found to be the following simple function:

$$\lambda_n = 460\sqrt{\Delta T} \quad (14)$$

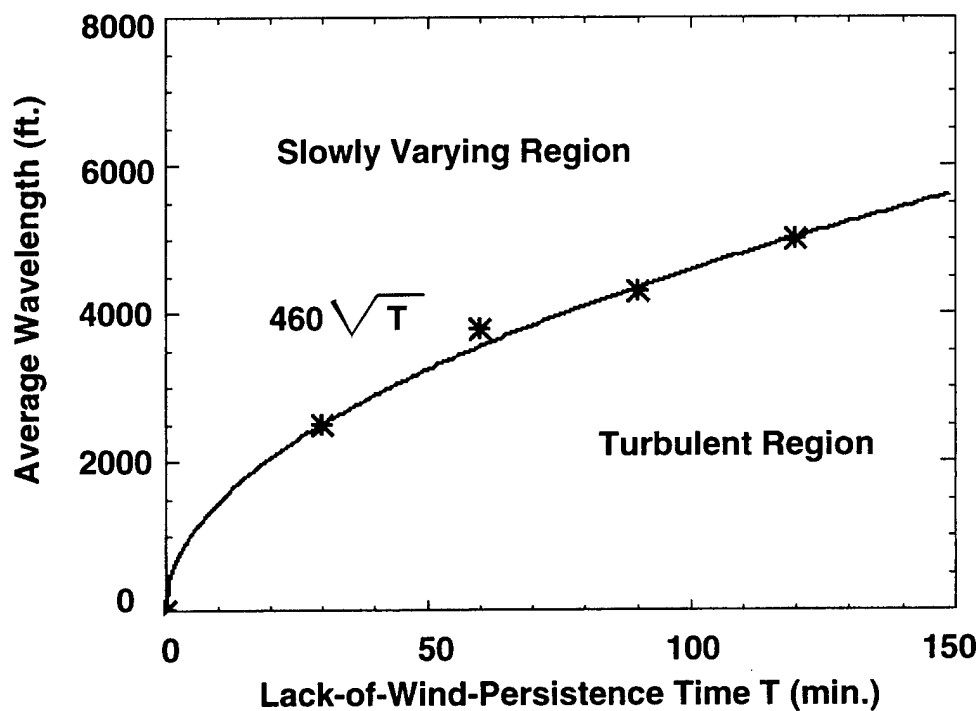


Figure 23. Average wavelength boundary separating the slowly-varying and turbulent components of winds as a function of elapsed time. Winds measured at the ER and WR during the months, December through April.

This curve identifies the average boundary wavelength, λ_B , in the measured wind, as a function of time interval in minutes prior to launch. The boundary wavelength defines the average boundary between the slowly-varying and the more rapidly-varying (turbulent) portions of the wind. On the average for a time interval, ΔT , wavelengths longer than λ_B are slowly varying while wavelengths shorter than λ_B are rapidly varying.

5. Potential Uses

The boundary wavelengths in Eq. (14) are necessary to develop empirical gust loads analysis forcing functions²⁰ and to establish loads due to atmospheric turbulence.^{21,22} Since the gust loads analysis accounts for the turbulent components of the winds statistically, and the average boundary between the slowly-varying and turbulent components of the wind can now be defined for the ER and WR ranges, there is the possibility of retaining in the day-of-launch loads analyses only those components of the winds that are slowly varying.²³ It is suggested that, to conservatively bracket the variation of this function, the values obtained with Eq. (14) be varied by an amount appropriate to the analysis being performed. A gust loads analysis in Refs. 20-21 is one such example.

6. Conclusions

This paper presented the results of work performed to determine the wavelength boundary between the slowly- and rapidly-varying components of the winds at the Eastern and Western ranges of the United States. Methodology was developed, and historical databases of winds were evaluated. Results include a simple function that relates the average boundary wavelength between slowly-varying and turbulent components in measured winds to the time interval before launch. It was shown that longer vertical wavelengths of wind profiles are more slowly varying over time than shorter wavelengths.

As a result of this work, it is now possible to identify in measured wind profiles, as a function of time prior to launch, the slowly-varying and the turbulent component of measured winds for two launch facilities. This information can be used to develop loads analyses utilizing only the appropriate portion of the wind. It is believed that for several launch vehicles this will represent a reduction in loads and, hence, higher launch availability without a reduction in predicted reliability.

References

1. Vail, J. R., "A Review of Space Vehicle Structural Design Problems During the Ascent Phase of Flight," TRW Report No. 09425-6001-R000, 18 March 1968.
2. Ryan, R. S., and King, A. W., "The Influential Aspects of Atmospheric Disturbances on Space Vehicle Design Using Statistical Approaches for Analysis," NASA TN D-4963, Jan. 1969.
3. Smith, O. E., and Adelfang, S. I., "On the Relationship Between Wind Profiles and the STS Ascent Structural Loads," AIAA 89-0709, Jan. 1989.
4. Adelfang, S. I., "Analysis of Jimsphere Wind Profiles Viewed in the Flight Time Domain of a Saturn Vehicle," J. Spacecraft, Vol. 7, No. 9, 1970, pp.1146-1149.
5. Smith, O. E., and Adelfang, S. I., "Wind Profile Models: Past, Present and Future for Aerospace Vehicle Ascent Design," AIAA-98-1047, Jan. 1998.
6. Luers, J., and Engler, N., "On Optimum Methods for Obtaining Wind Data from Balloon Sensors," Journal of Applied Meteorology, Vol. 6, 1967, pp. 816-823.
7. Fleming, E. R., "Spacecraft and Launch Vehicle Loads," Vol. I, Chapter 6, Flight Vehicle Materials, Structures, and Dynamics, American Society of Mechanical Engineers, March 1991.
8. Kabe, A. M., "Design and Verification of Launch and Space Vehicle Structures," AIAA-98-1718, April 1998.
9. Macheske, V. M., Womack, J. M., and Binkley, J. F., "A Statistical Technique for Combining Launch Vehicle Atmospheric Flight Loads," AIAA 93-0755, Jan. 1993.
10. Womack, J. M., and Binkley, J. F., "A Statistical Technique for Combining Launch Vehicle Loads During Atmospheric Flight," Aerospace Report TOR-0091(6530-06)-2, 30 Aug. 1992.
11. Spiekermann, C. E., and Kabe, A. M., "Statistical Combination of Launch Vehicle Gust and Buffet Atmospheric Flight Loads," AIAA-98-2010, April 1998.
12. Binkley, J. F., Clark, J. B., and Spiekermann, C. E., "An Improved Procedure for Combining Atmospheric Flight Loads on the Day of Launch," AIAA 99-1254, April 1999.
13. Meirovitch, L., Elements of Vibration Analysis, 2nd ed., McGraw-Hill Publishing Company, 1986, pp. 238-240.
14. Bendat, J. S., and Piersol, A. G., Random Data Analysis and Measurement Procedures, 2nd ed., Wiley-Interscience, N.Y., 1986, p. 409.
15. Luers, J. K., and MacArthur, C. D., "Ultimate Wind Sensing Capabilities of the Jimsphere and Other Rising Balloon Systems," NASA CR-2048, June 1972.

16. Johnson, D. L., and Vaughan, W. W., "Sequential High-Resolution Wind Profile Measurements," NASA, Tech. Paper 1354, Dec. 1978.
17. Adelfang, S. I., Ashburn, E. V., and Court, A., "A Study of Jimsphere Wind Profiles as Related to Space Vehicle Design and Operations," NASA CR-1204, Nov. 1968.
18. Wilfong, T., Smith, S., and Crosiar, C. L., "Characteristics of High-Wind Profiles Derived from Radar-Tracked Jimsphere and the Rose Processing Program," Journal of Atmospheric and Oceanic Technology, Vol. 14, 1997, pp. 318-325.
19. Hoel, P. G., Port, S. C., and Stone, C. J., "Introduction to Statistical Theory," Houghton Mifflin Company, Boston, 1971, pp. 174-178.
20. Sako, B. H., Kim, M. C., and Kabe, A. M., "Derivation of Forcing Functions for Monte Carlo Atmospheric Gust Loads Analysis," AIAA 99-1251, April 1999.
21. Kim, M. C., Kabe, A. M., and Lee, S. S., "Atmospheric Flight Gust Loads Analysis," AIAA 99-1252, April 1999.
22. Clark, J. B., Kim, M. C., and Kabe, A. M., "Statistical Analysis of Atmospheric Flight Gust Loads Analysis Data," AIAA 99-1253, April, 1999.
23. Kabe, A. M., Spiekermann, C. E., Kim, M. C., and Lee, S. S., "A Refined and Less Conservative Day-of-Launch Atmospheric Flight Loads Analysis Approach," AIAA 99-1255, April 1999.